In-Situ Determination of Precipitation Kinetics During Heat Treatment of Superalloy 718

Jonathan Cormier, P. Gadaud, M. Czaplicki, R y Zhang, H B Dong, T M Smith, F Zhang, J S Tiley, S L Semiatin

In-Situ Determination of Precipitation Kinetics During Heat Treatment of Superalloy 718

J. CORMIER, P. GADAUD, M. CZAPLICKI, R.Y. ZHANG, H.B. DONG, T.M. SMITH, F. ZHANG, J.S. TILEY, and S.L. SEMIATIN

Two *in-situ* test techniques were used to obtain insight into the isothermal precipitation kinetics of γ'' and γ' in superalloy 718. The first method consisted of measurements of Young's modulus using a dynamic-resonance method (DRM), and the other comprised determination of the evolution of the lattice parameter of the γ-matrix phase *via* neutron diffraction. For both techniques, solution-treated-and-water-quenched samples were heated to a nominal test temperature of 923 K, 953 K, 1013 K, or 1053 K and held for a time of ~ 5 to 50 hours, at the end of which a near-steady condition in terms of an apparently-constant modulus/lattice parameter had been achieved. The observations from each test technique suggested sequential periods of rapid initial increase in volume fraction followed by a gradually-decreasing rate of change. The data were converted to transformed fraction as a function of time and interpreted in terms of phenomenological (JMAK) and mechanistic (nucleation-and-growth) models. From the former approach, Avrami exponents which decreased from approximately unity at the lower two temperatures to ~ 0.5 at the highest temperature, were deduced. The transformed fraction-versus-time behaviors were well replicated using fast-acting numerical simulations based on the mechanistic model. These simulations highlighted the competition between nucleation and growth in determining overall transformation kinetics.

https://doi.org/10.1007/s11661-020-06078-4

I. INTRODUCTION

FOR many years, superalloy 718 has been the workhorse material for moderate-temperature applications in the aero-engine and power-generation industries. Combining an attractive blend of low cost, ease of manufacture with respect to both mill products and finished components, and balance of properties, 718 has accounted for ~ 50 pct of the total superalloy market since it was first introduced in the early 1960s.[1–3] The use of the alloy has declined somewhat in recent years due to the need for higher-temperature capability as well as the development of new, moderate-cost, cast-and-wrought γ–γ' superalloys with higher strength.[4] Nevertheless, the widespread use of 718 and the absence of proprietary restrictions have promoted extensive research to understand its physical metallurgy, let alone have its formulation and processing methods serve as the basis for emerging, modern alloys.[5]

One of the key attributes of 718 includes its ability to be heat treated uniformly for thick-section hardware and its good weldability. In part, these attributes are associated with the moderate aging temperatures and the somewhat sluggish precipitation kinetics of its two ordered strengthening phases, both of which have a nominal composition of Ni_3X. These phases are the metastable DO_{22} bct γ'' (for which X is primarily Nb with lesser amounts of Ti and Al) and stable $L1_2$ fcc-like γ' (for which X consists of comparable amounts of Al, Ti, and Nb). To optimize strength, 718 components are usually solution treated just below or above the solvus temperature of the stable DO_a orthorhombic δ phase (which provides grain-size control), oil quenched, and then given a two-step aging treatment at 993 K and then 893 K. By this means, a uniform dispersion of ellipsoidal γ'' and spheroidal γ' precipitates with diameters of ~ 20 to 30 or ~ 10 to 20 nm, respectively, and a total volume fraction of ~ 15 pct is produced. Aging immediately following hot forging without an intermediate solution treatment, or so-called direct-aging, has also been

J. CORMIER, P. GADAUD, and M. CZAPLICKI are with the Institut Pprime, UPR CNRS 3346, ISAE-ENSMA, 1 avenue Clément Ader, BP 40109, 86961 Futuroscope-Chasseneuil Cedex, France. Contact e-mail: jonathan.cormier@ensma.fr R.Y. ZHANG is with the Open University, Milton Keynes MK7 6AA, UK. H.B. DONG is with the University of Leicester, Leicester LE1 7RH, UK. T.M. SMITH is with the NASA Glenn Research Center, Cleveland, OH 44135. F. ZHANG is with the CompuTherm LLC, Middleton, WI 53562. J.S. TILEY and S.L. SEMIATIN are with the Materials and Manufacturing Directorate, Air Force Research Laboratory, Wright-Patterson Air Force Base, OH 45433.

Manuscript submitted August 5, 2020; accepted October 19, 2020.

Published online: 13 November 2020

applied to further refine the precipitate structure and obtain higher levels of strength.[6]

Because of the industrial importance of 718, a number of attempts have been made to quantify its aging response *via* the determination of both isothermal and continuous-cooling transformation diagrams.[7–13] A comparison of these measurements has revealed wide variations, some of which can be attributed to difficulties in resolving the fine strengthening phases and their volume fractions as well as the effect of relatively-small variations in alloying-element content (especially Nb), which are still within the nominal alloy specification, on overall phase equilibria.[14,15] For example, volume fractions reported in the literature for heat-treated 718 have varied from approximately 4 to 15 pct for γ'' and from 4 to 18 pct for and γ'.[16–20]

Challenges in characterizing the very fine microstructure typically formed in solution-treated-and-aged 718 *via* transmission or high-resolution-scanning electron microscopy and atom-probe tomography have spurred the development of other approaches to understand/quantify phase-transformation kinetics. These include non-destructive evaluation (*in-situ*) methods such as electrical resistivity, various ultrasonic methods, neutron diffraction (*e.g.*, to determine the temporal evolution of lattice parameters under isothermal conditions[21]), and differential thermal analysis (*e.g.*, to establish the onset of precipitation or dissolution of γ'', γ', and δ during heating and cooling[22,23]). Alternatively, several attempts have been made to develop modeling-and-simulation techniques which treat the detailed mechanisms of nucleation, growth, and coarsening of the precipitate phases in 718 (as well as related alloys such as 625 and 718Plus).[24–28] These approaches require large amounts of thermodynamic and kinetic input data and often include simplifying assumptions or calibration/tuning methods whose bases need to be justified. Despite such shortcomings, the tools provide great promise for investigating the effect of changes in processing parameters on heat-treatment response, microstructure variability in large forgings, *etc.*

The objectives of the present work were to establish the feasibility of applying novel/indirect *in-situ* measurement techniques to track the evolution of precipitation in superalloy 718 and to interpret the measurements *via* comparison with both a JMAK (phenomenological) model and fast-acting simulations that describe the nucleation-and-growth stages of the aging process. For this purpose, two separate series of isothermal aging experiments were performed: one based on measurement of Young's modulus using a dynamic-resonance method (DRM)[29–32] and the other comprising neutron diffraction to quantify changes in the lattice parameter of the γ matrix.

II. MATERIALS AND EXPERIMENTAL PROCEDURES

A. *Materials*

Two lots of superalloy 718 with almost identical composition (Table I), as determined by standard spectrographic and X-ray fluorescence methods, were used to establish the efficacy of *in-situ* techniques for quantifying aging response.

The first lot, used for DRM, was received in the form of a sub-δ-solvus hot forging having a uniform γ grain size of ~ 10 μm (corresponding to ASTM 10). A section of the forging was super-δ-solvus solution treated at 1373 K for 1 hour and water quenched (cooling rate ~ 100 K/s), thereby producing a microstructure comprising single-phase γ grains with an average circle-equivalent diameter of 300 to 400 μm (ASTM 0-1). DRM samples in the form of prismatic beams measuring $30 \times 5 \times 1.5$ mm^3 were extracted from the heat-treated section *via* electrical-discharge machining followed by polishing to a mirror-like finish.

The 718 material used for neutron-diffraction experiments was extracted from a forged bar. Rods measuring 8-mm diameter were machined *via* lathe turning and were heat treated below the δ solvus at 1273 K for 1 hour followed by fan cooling (cooling rate ~ 4 K/s). This heat treatment produced a small fraction (~ 0.01) of δ phase which pinned the γ grain boundaries, yielding an average γ grain size of 30 μm.

B. *DRM Experiments*

DRM was conducted at Institut Pprime in France to gage the kinetics of precipitation *via* measurements of the Young's modulus. To this end, solution-treated samples were tested in a home-made system[29] which included an indirect-resistance vacuum furnace. Within this system, experiments can be performed under high vacuum (10^{-4} Pa) at temperatures from 150 K to 1400 K without any harmful contact, the sample being maintained horizontally between steel wires located at the vibration nodes. In the present work, each sample was heated at a rate of 2 K/min to one of four nominal aging temperatures (923 K, 953 K, 1013 K, or 1053 K), and held isothermally for total times ranging from 6 to 47 hours, the exact duration depending on aging kinetics. After an initial 5-minute soak at the test temperature, modulus measurements were made at a series of time intervals. Under the chosen test conditions, γ'' and γ' precipitates, but no δ-phase needles, were formed.

The modulus measurements, performed per ASTM International standard E1875-13,[32] were based on the bending vibration of a beam specimen under continuous frequency excitation. Excitation and detection in the test apparatus were effected by an electrostatic device based on the capacitance between the test sample and a special electrode. The longitudinal Young's modulus E of a bulk beam sample in a bending mode is determined using the following relation:

$$E = 0.9464\rho F^2 \frac{L^4}{h^2} T\left(\frac{h}{L}, \upsilon\right), \qquad [1]$$

where F is the resonant frequency, ρ is the density, υ is Poisson's ratio, h and L are the beam thickness and length, respectively, and T(h/L,υ) is a shear-correcting factor close to unity. For homogeneous materials, the

Table I. 718 Compositions (Weight Percent)

Material	Fe	Cr	Mo	Nb	Ti	Al	Co	Ni
DRM	17.5	17.9	2.92	5.42	1.01	0.49	0.37	bal
Neutron Diff	18.0	18.1	2.90	5.42	0.91	0.48	0.37	bal

intrinsic accuracy is about ±0.5 pct at room temperature. The prime sources of error are associated with uncertainty in sample dimensions and density.

Relative to the more conventional impulse technique,[32] continuous frequency excitation enables real-time follow-up on the screen of a network analyzer of the resonance frequency with an accuracy of ± 0.1 Hz. Consequently, a change in resonant frequency of the order of 0.5 Hz (due to an increase/decrease in temperature or a change in microstructure at a fixed temperature, for example), is indicative of a change in modulus. In particular, a change of 0.5 Hz corresponds to a variation of Young's modulus of ~ 15 MPa for the moduli of nickel-base superalloys such as 718.

The temporal variation in moduli (E) were assumed to be related to the volume fraction (f) of precipitates that evolved during aging per the rule of mixtures, *i.e.*,

$$E_{alloy} = E_{\gamma},\ f_{\gamma} + E_{\gamma''}f_{\gamma''} + E_{\gamma'}f_{\gamma'}, \qquad [2a]$$

where the subscripts denote the γ matrix, the bct γ'' precipitates, and the fcc γ' precipitates. Unfortunately, there are very few measurements in the literature of the high-temperature elastic constants for the separate phases. In one report, it has been suggested that the elastic constants of γ and γ'' are within 1 pct of each other.[33] In another investigation, the shear modulus of Ni_3Al (~ γ') was suggested to be ~ 1 to 8 pct higher than that of the disordered γ phase.[34] In the present work, to avoid possible ambiguity, the precipitates were thus treated in a "homogenized" sense, such that Eq. [2a] becomes the following:

$$E_{alloy} = E_{\gamma}f_{\gamma} + E_{p}f_{p} = E_{\gamma}(1 - f_{p}) + E_{p}f_{p} \qquad [2b]$$

in which E_p and f_p represent the "homogenized" precipitate modulus and total volume fraction of precipitate. Solving for f_p in Eq. [2b] yields the following relation:

$$f_{p} = (E_{alloy} - E_{\gamma})/(E_{p} - E_{\gamma}) \qquad [3]$$

When there is no precipitate, $E_{alloy} = E_{alloy_o} = E_{\gamma}$. The ratio of the instantaneous fraction of precipitate to the maximum amount f_{pmax} (at the conclusion of precipitation) is then simply:

$$f_{p}/f_{pmax} = \left(E_{alloy} - E_{alloy_o}\right)/\left(E_{alloy_{max}} - E_{alloy_o}\right) \qquad [4]$$

In other words, the fractional change in precipitate volume fraction is assumed to be linearly related to the fractional change in Young's modulus.

To supplement the DRM observations for isothermal testing of solution-treated samples, the Young's modulus of an additional sample that had been initially supersolvus solution treated and given a "standard" aging treatment (993 K/8 hours + 893 K/ 8 hours) was determined *via* DRM at a series of progressively increasing temperatures.

C. *Neutron-Diffraction Experiments*

Neutron diffraction experiments were conducted using the ENGIN-X time-of-flight diffractometer at the ISIS spallation neutron source in the UK.[35] Detailed experimental procedures are contained in Reference 21. As in this prior work, test samples in the present effort were heated in air in a radiant furnace from room temperature to either 953 K or 1053 K in approximately 10 minutes and soaked at temperature for an additional 5 minutes prior to commencing diffraction measurements. The measurements were conducted using a 4 × 4 × 4 mm^3 volume of material and an acquisition time of ~ 5.5 minutes per datum. Tests were performed for total times of 15.4 or 11.7 hours at the lower or higher temperatures, respectively. During such a hold time, a thin surface oxide, whose thickness ($\ll$50 μm) comprised a negligible fraction of the irradiated volume, was formed.

The average lattice parameter of the γ matrix phase was determined from the diffraction spectra by applying a Pawley-type refinement *via* the GSAS program in the OpenGenie software package. Similar to the approach used to reduce the DRM results, the fractional change in the γ-matrix lattice parameter, $\Delta a_{\gamma}/a_{\gamma}$, was assumed to be linearly proportional to the volume fraction of precipitate f_p.[36,37] When the misfit is due to a thermal effect, the following relation applies:

$$\frac{\Delta a_{\gamma}}{a_{\gamma}} = \frac{4\mu_{\gamma}C_6\varepsilon}{3K_{\gamma}(1+\varepsilon)^3}f_{p} \qquad [5a]$$

In Eq. [5a], μ_{γ} and K_{γ} are the shear modulus and bulk modulus of the γ matrix, respectively, and ε is the *linear* misfit strain (~ cube root of the volumetric strain). C_6 is equal to the quotient $3K_p/(3K_p + 4\mu_{\gamma})$ in which K_p is the bulk modulus of the precipitate. An alternate form of Eq. [5a] for the fractional change in overall lattice parameter has been suggested for the case of lattice misfit due to a phase transformation in which the precipitates are coherent with the matrix, or a situation more appropriate in the present work,[36,37] *i.e.*,

$$\frac{\Delta a_\gamma}{a_\gamma} = \frac{C_6 \varepsilon}{C_7 (1+\varepsilon)^3} f_p, \qquad [5b]$$

where C_7 is equal to $3K_\gamma/(3K_\gamma + 4\mu_\gamma)$.

Once again, assuming that the factor multiplying fp on the right-hand side of Eqs. [5a] or [5b] is constant, the ratio of the instantaneous fractional change in lattice parameter to the final, maximum change may be taken to be equal to f_p/f_{pmax}. Furthermore, in the present work, the change in lattice parameter of the γ phase is assumed to be largely related to the precipitation of γ'' because of its large misfit. The γ–γ'' misfit is approximated here by an overall volume change that does not differentiate the dilational and tetragonal contributions. Such an assumption may be acceptable for distances at least several precipitate diameters away from the particles themselves and/or small volume fractions of precipitate. The misfit between the γ and γ' phases, on the other hand, is very small, and the precipitation of γ' was thus assumed to have a negligible effect on the evolution of the matrix lattice parameter.

Uncertainty in the magnitude of the γ lattice parameter (~ ±0.0002 Å) was associated with the fitting of diffraction spectra *via* the Pawley refinement procedure.

III. RESULTS

The principal results of the present investigation consisted of measurements of the temporal variation of the sample (Young's) modulus and the lattice parameter of the γ matrix at the various test temperatures.

A. *DRM Measurements*

The DRM measurements provided insight into the broad variation of Young's modulus (E_{alloy}) with time and overall precipitation kinetics. In general, the initial modulus (at time t ~ 0), showed the expected decrease with increasing temperature (Figure 1(a)). The only noticeable exception to this trend appeared to be exhibited by the data for 1013 K. This observation was perhaps a result of the very rapid increase in E_{alloy} at short times at this temperature which was not captured fully in the experiments.

When the modulus data were recast in terms of Eq. [4], the temperature and time dependence of what were hypothesized to be precipitation kinetics became apparent (Figure 1(b)). At all temperatures, the value of f_p/f_{pmax} showed an initial rapid increase with time followed by a much slower rate at long times resulting in an asymptotic approach to the value of unity. For all test temperatures, a finite incubation (nucleation) time appeared to be absent. This observation may be a result of very rapid nucleation during the heating transient to the test temperature (whose effect on the observations is discussed in the Appendix) or the short soak period required for temperature equilibration of the test system prior to the first measurement (*i.e.*, ~ 5 minutes). Despite this possible limitation of the test method, the results in Figure 1(b) do indicate a marked temperature dependence reminiscent of classical isothermal-transformation (IT) behavior. Specifically, the kinetics were comparatively slow at the two lower test temperatures (923 and 953 K), most rapid at the intermediate temperature of 1013 K and just moderately slower than

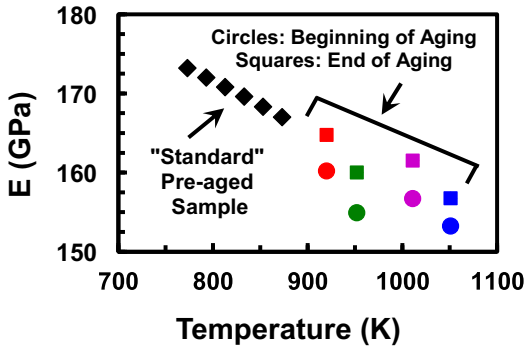

Fig. 2—Comparison of measurements of Young's modulus for solution-treated-and-isothermally-aged samples and a specimen that was given a "standard" two-step aging treatment prior to DRM at a series of temperatures.

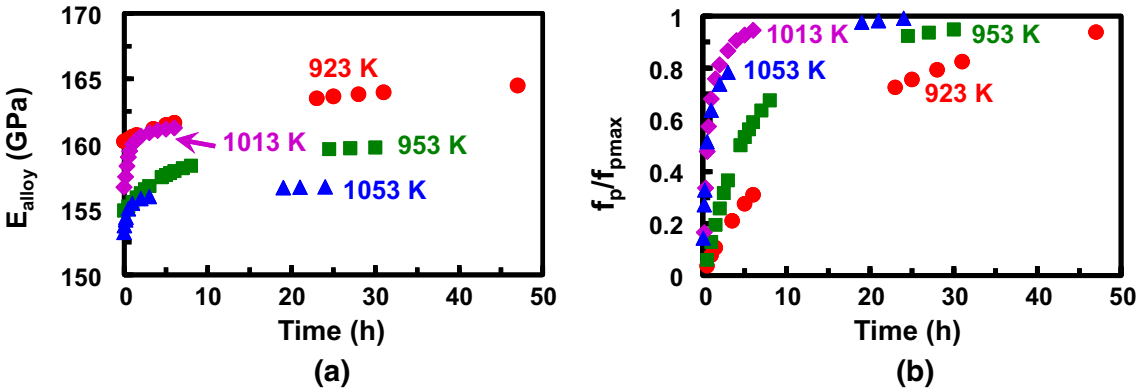

Fig. 1—DRM results for super-δ-solvus solution-treated 718: (*a*) Measurements of the Young's modulus as a function of time and temperature and (*b*) the corresponding precipitation kinetics calculated per Eq. [4].

this at the highest temperature (1053 K). Hence, the "nose" of the IT curve was likely located very near 1013 K.

The hypothesis that changes in modulus during isothermal-hold trials were due to precipitation was confirmed, at least to a first order, by comparing the isothermal results to the measurements for the sample that was initially given the "standard" two-step aging treatment (993 K/8 h + 893 K/8 h) to produce a near-equilibrium aged structure and then DRM tested at various temperatures (Figure 2). Although there is some data scatter, modulus-*vs*-temperature trends for the pre-aged condition and the long-time isothermal experiments do indeed follow a similar trend. To a certain degree, the comparison highlights the benefit of *in-situ* tests which avoid uncertainties associated with trying to assess differences in behavior of separate samples whose moduli are of comparable magnitude.

The DRM observations were interpreted more fully in terms of Avrami plots and nucleation-and-growth simulations. These analyses are discussed in Section IV.

B. *Neutron-Diffraction Measurements*

The neutron-diffraction measurements 953 and 1053 K complemented the DRM observations. At both test temperatures, the lattice parameter for the γ matrix showed an exponential-like behavior as a function of time, which was characterized by initially-sharp decrease followed by a relatively slow rate of decrease before an asymptotically approach a steady-state or near-steady-state value (Figure 3(a)). (As shown in the figure for the experiment at 953 K, an exponential curve was fit to the measurements to obtain the long-time (50 hours)/"equilibrium" lattice parameter, *i.e.*, 3.6385 Å). In view of the limited misfit between the γ and γ' phases, the observed decrease can likely be ascribed primarily to the precipitation of γ'' which has a large positive misfit with the matrix.

As for the DRM results, the change in lattice parameter normalized by the maximum change (= initial value minus the final/equilibrium value) showed a noticeable effect of test temperature on behavior (Figure 3(b)). Once again, the apparent aging kinetics at 1053 K were substantially more rapid than those at 953 K. Moreover, the DRM and neutron-diffraction data for 953 and 1053 K (plotted together in Figure 4) presented no discernible trend with regard to differences.

IV. DISCUSSION

The DRM and neutron-diffraction measurements were interpreted in the context of prior observations, phenomenological (Avrami) fits to the data, and simulation predictions using a nucleation-and-growth model.

A. *Comparison with Prior Observations*

The applicability of the DRM method for quantifying precipitation kinetics was verified by comparison to prior direct measurements of the evolution of precipitate volume fraction in 718 as a function of time, as determined by Han.[16] As in the present work, the former data were obtained for samples that had been super-δ-solvus solution treated and water quenched before aging. By contrast, Han's aging experiments comprised nominally-isothermal furnace heat treatment

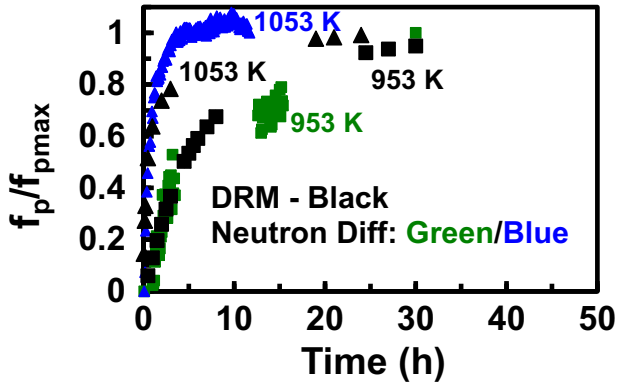

Fig. 4—Comparison of precipitation kinetics at 953 K and 1053 K estimated from DRM and neutron diffraction.

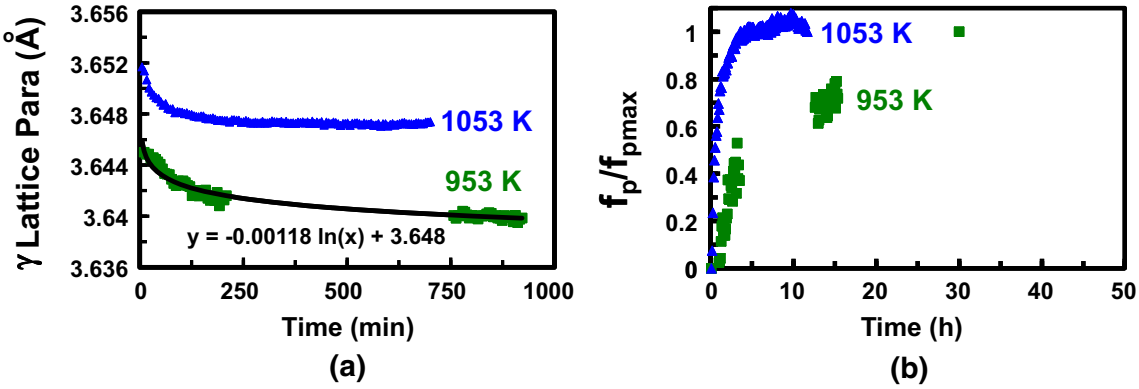

Fig. 3—Temporal evolution of the (*a*) γ-matrix lattice parameter and (*b*) estimated precipitation kinetics during isothermal heat treatment of a solution-treated 718 sample at 953 K and 1053 K.

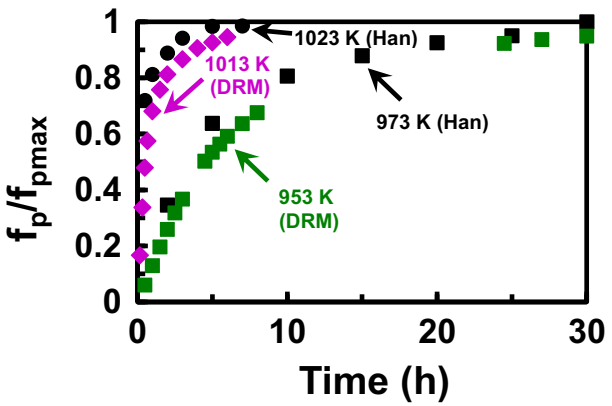

Fig. 5—Comparison of precipitation kinetics in terms of normalized volume fractions measured by Han[16] and those deduced from DRM measurements.

of (encapsulated) 0.2-mm thick strips, whose heat-up time was very short (~ 15 seconds to reach a temperature within 5 K of the furnace temperature). To avoid the possibly-confounding influence of small lot-to-lot variations in alloy composition on the absolute volume fraction and type of precipitates and to enable comparison with the DRM data, the measured total ($\gamma'' + \gamma'$) volume fractions were normalized by the measured long-time ("equilibrium") fraction of precipitate. The comparison revealed that the DRM measurements at 953 K and 1013 K were very similar to those of Han determined for aging temperatures of 973 K and 1023 K (Figure 5). In particular, the DRM values for 953 K and 1013 K showed slightly slower kinetics than Han's values for 973 K and 1023 K, respectively. This behavior would be expected if the nose of the isothermal-transformation curve(s) lay closer to 1023 K than the temperature of 1013 K as suggested by the examination of the DRM data alone. The difference may have also arisen from differences in the composition of the two lots of 718.

In view of the good agreement shown in Figure 5, it may be concluded that DRM-modulus data do indeed indicate a real difference in the magnitude of the Young's modulus of the γ matrix and precipitate ($\gamma'' + \gamma'$) phases. Assuming an (average) difference in modulus between the un-aged and fully-aged conditions to be 4.5 GPa (Figure 2) and the total volume fraction of precipitate to be ~ 0.15,[16,17,20] the modulus of the precipitates was estimated using Eq. [2b] to be 186 GPa, or approximately 30 GPa greater than that of the matrix. This value is considerably greater than those suggested in prior work.[33,34]

Although the neutron-diffraction lattice-parameter measurements were likely an indication of the precipitation of γ'' primarily (with its much larger misfit relative to that of γ'), the normalized data were very similar to those obtained *via* DRM (Figure 4) and thus Han's direct volume-fraction measurements.[16]

An assessment was also made to determine if the neutron-diffraction results could be rationalized on the basis of Eqs. [5a] or [5b]. The fractional change in the γ lattice parameter ($\Delta a_\gamma/a_\gamma$) measured at (or determined by extrapolation to) long time was either ~ 0.00178 or ~ 0.00137 for the experiments at 953 K and 1053 K, respectively.

Assuming a Poisson ratio υ of 0.3 for both the matrix and precipitate phases, Young's moduli E as determined/deduced from the DRM results, and the bulk modulus K to be equal to $E/(3(1 - 2\upsilon))$, inputs to Eqs. [5a] and [5b] comprised μ_γ = 61.5 GPa, K_γ = 133 GPa, $K_p = K_{\gamma'} = 155$ GPa, a linear misfit strain ε = 0.0148 (based on a volume difference of 4.5 pct[26]), and $f_{\gamma''} = 0.11$ (953 K) or 0.095 (1053 K). The corresponding predicted magnitudes of $\Delta a_\gamma/a_\gamma$ were thus 0.000626 (953 K) and 0.000541 (1053 K) using Eq. [5a] or 0.00164 (953 K) and 0.00142 (1053 K) using Eq. [5b]. Hence, the predictions using Eq. [5b] showed reasonably good agreement with the measurements, but those derived from Eq. [5a] were low by a factor of ~ 2.5. This trend is not surprising in view of the fact that Eq. [5b] is more pertinent to predict the lattice misfit strain associated with phase transformation, *i.e.*, the precipitation of γ'' in superalloy 718. The good agreement between the measurements and Eq. [5b] may also be partly related to the large sample volume probed during neutron diffraction, the fitting of multiple diffraction peaks, and the likely presence of all three γ'' variants in each γ grain, all of which taken together would tend to minimize directionality associated with local tetragonality.

B. *JMAK Analysis*

The precipitation kinetics deduced from the DRM measurements were re-cast in the form of the classical JMAK relation derived by Johnson, Mehl, Avrami, and Kolmogorov[38–42] for phase transformation controlled by nucleation and growth processes:

$$X = 1 - \exp(-kt^n) \qquad [6a]$$

$$\text{or, } \log[-\ln(1 - X)] = n \log t + \log k \qquad [6b]$$

In these equations, X is the transformed fraction, k and n are material- and temperature-dependent constants, and t denotes time. The exponent (n) is usually determined from so-called Avrami plots of log [−ln (1 − X)] versus log t. In the present work, X was taken to be the normalized volume fraction of precipitate (*i.e.*, f_p/f_{pmax}), thus yielding the trends shown in Figure 6. At the two lower temperatures (923 K and 953 K, Figures 6(a) and (b), the Avrami exponent was close to unity (*i.e.*, ~ 0.91). At the next higher temperature, 1013 K, the plot (Figure 6(c)) suggested a continuously decreasing slope from ~ 1 at low transformed fractions (corresponding to low values of log [−ln (1 − X)]) to ~ 0.5 at the end of transformation. Finally, the Avrami exponent assumed an approximately constant value of ~ 0.5 at the highest test temperature (1053 K, Figure 6(d)). The variation of Avrami exponent with aging temperature may be hypothesized to be due kinetics which are most strongly influenced by nucleation at lower temperatures (at which diffusional growth

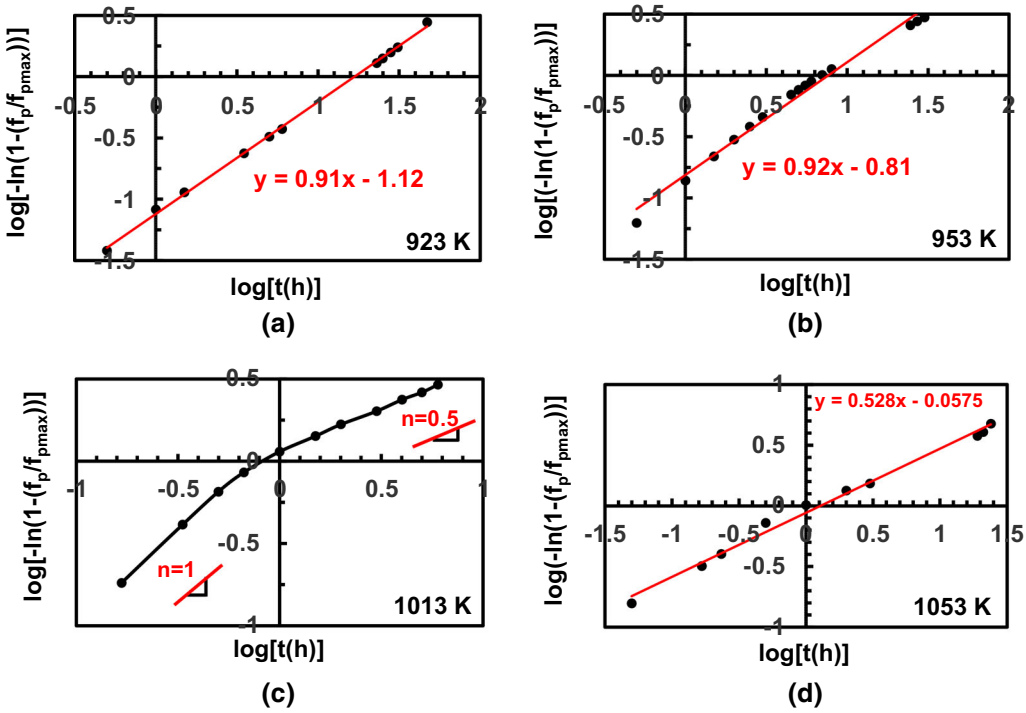

Fig. 6—Avrami plots of precipitation kinetics deduced from DRM measurements at (*a*) 923 K, (*b*) 953 K, (*c*) 1013 K, and (*d*) 1053 K.

Table II. Key Input Parameters for Nucleation-and-Growth Simulations

Parameter	Baseline Dataset	Modified-Baseline Dataset
γ''–γ Interface Energy (mJ/m^2)	56	62.3
γ'–γ Interface Energy (mJ/m^2)	40	40
Thermodynamic Factor, Nb (−)	1.94	1.1
Thermodynamic Factor, Ti (−)	1.3	1.3
ΔG_{el} for γ''–γ Misfit (MPa)	12	70
Effective Diffusivity of Cr (m^2/s)	4.57×10^{-5} Exp(−34280/T)	4.57×10^{-5} Exp(−34280/T)
Effective Diffusivity of Al (m^2/s)	3.94×10^{-4} Exp(−34280/T)	3.94×10^{-4} Exp(−34280/T)

T denotes temperature in Kelvins.

of precipitates is sluggish) and by diffusion growth with lower nucleation rates at higher temperatures. However, it should be emphasized that the JMAK approach should be viewed as qualitative in nature for the complex aging behavior of 718, thus mandating the need for mechanism-based analysis.

C. *Nucleation-and-Growth (N&G) Analysis*

Because of the difficulty in assigning a physical basis for changes in the Avrami exponent with temperature, a series of numerical simulations was performed to describe the interaction of concurrent nucleation and growth of γ'' and γ' precipitates. For this purpose, a fast-acting-simulation routine based on the Kampmann-and-Wagner formalism[43] was utilized. The model formulation underlying the simulations, various pieces of input data, and the calculation procedures are described in a companion paper.[44] In brief, it is assumed that precipitates are formed by homogeneous nucleation and grow by diffusion. For superalloy 718, it was concluded that nucleation is controlled by the partitioning of niobium or titanium and growth is limited by chromium or aluminum for γ'' and γ', respectively. Some of the key input parameters for the simulations (in terms of both a baseline dataset and a modified baseline dataset) are summarized in Table II; others, such as the assumed phase compositions, equilibrium volume fractions, *etc*. can be found in Reference 44.

Predictions of the normalized $\gamma'' + \gamma'$ volume-fraction dependence on time (*i.e.*, f_p/f_{pmax} *vs* t) from the simulations showed very good to excellent agreement with experimental values deduced from DRM (Figure 7). Predictions using the baseline and modified-baseline input datasets (black and red curves, respectively, in Figure 7) were similar. The largest difference was for the predicted behaviors at 923 K, with the modified-baseline input dataset showing better agreement with DRM measurements. The sensitivity of

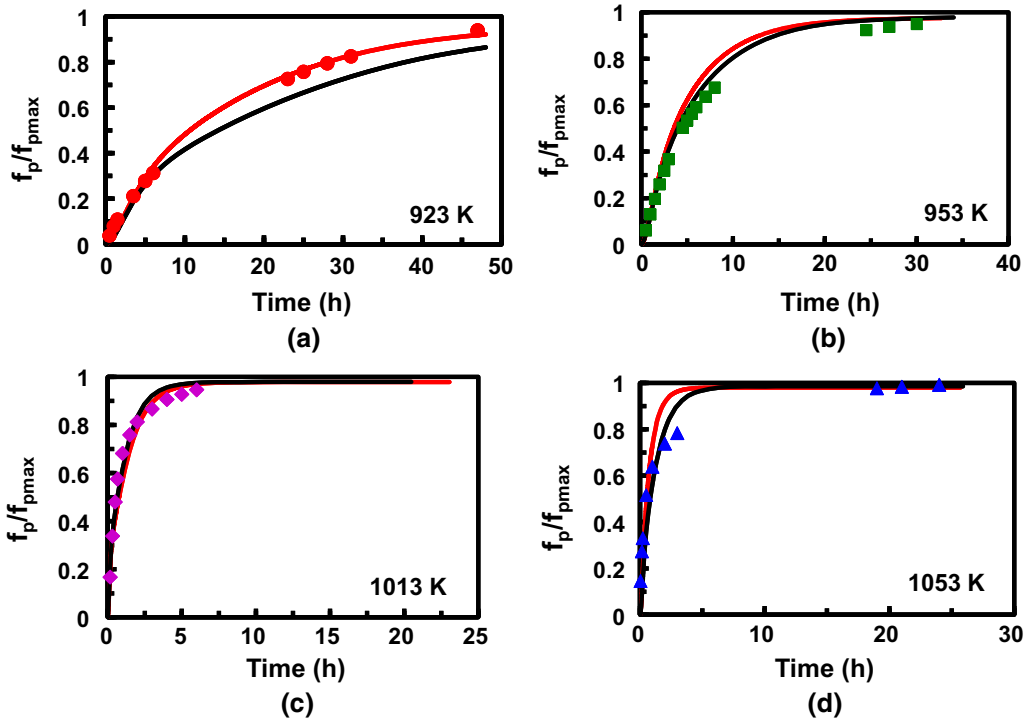

Fig. 7—Comparison of precipitation kinetics in terms of normalized total volume fractions of γ'' and γ' (f_p/f_{pmax}) deduced from DRM (data points) and simulation predictions using the baseline (black lines) or modified-baseline (red lines) input datasets for aging temperatures of (*a*) 923 K, (*b*) 953 K, (*c*) 1013 K, and (*d*) 1053 K (Color figure online).

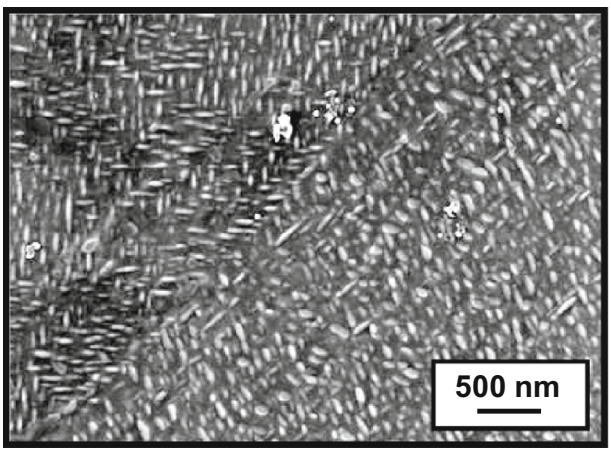

Fig. 8—SEM image of the microstructure developed during aging of 718 in the DRM experiment performed at 1053 K.

the predictions to various inputs is discussed further in Reference 44. As discussed in the Appendix, N&G simulations which included the specific heating ramp to the peak temperature suggested, however, that the neglect of this transient did not substantially change the agreement between N&G predictions and the DRM measurements except for the results at the highest temperature (1053 K).

Detailed inspection of the simulation predictions for the DRM experiments also revealed that nucleation was essentially complete by values of f_p/f_{pmax} equal to approximately 0.21, 0.22, 0.17, and 0.13 for temperatures of 923 K, 953 K, 1013 K, or 1053 K, respectively. Although the variation in the values of this volume fraction are not very large, they perhaps suggest that the change in Avrami exponent with increasing temperature (Figure 6) is a result of a transition from nucleation-dominated to growth-dominated precipitation. Such a concept is often used to explain the commonly-observed C shape of IT diagrams.

The N&G analysis (in conjunction with measured/predicted coarsening rates[44,45]) was also useful in the prediction of the final microstructures developed during the DRM experiments. An example micrograph for the experiment at 1053 K is shown in Figure 8. In this instance, the 2D diameters of the disk-like γ'' and spheroidal γ' precipitates were 132.3 ± 16.3 nm and 67.3 ± 8.8 nm, respectively. Taking into account the accelerated rate of coarsening of γ'' associated with the loss of coherency with the γ matrix with increasing size,[45,46] simulation-predicted diameters were ~ 123 nm (for γ'') and ~ 55 nm (for γ') at the end of the 24-hour aging time (~ 4 hours for N&G followed by ~ 20 hours during which static coarsening occurred). For the microstructure developed at 1013 K (not shown herein), the measured precipitate diameters were 30.2 ± 6.4 nm (γ'') and 12.1 ± 2.6 nm (γ'). The corresponding simulation predictions were 28 and 16 nm, respectively. Although relatively minor, the differences between measured and predicted sizes may be ascribed to the experimental difficulty in SEM imaging of very fine precipitates (especially for γ'), stereological considerations (*i.e.*, the 3D nature of the simulations versus the 2D

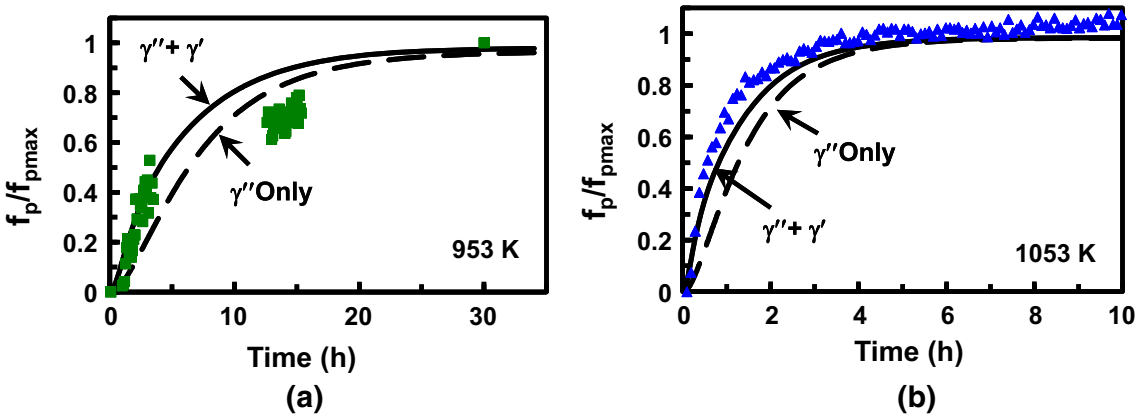

Fig. 9—Comparison of precipitation kinetics in terms of normalized volume fraction of precipitate (f_p/f_{pmax}) deduced from neutron diffraction (data points) and simulation predictions using the baseline input dataset (black lines) for an aging temperature of (*a*) 953 K or (*b*) 1053 K. The simulations results correspond to γ'' alone (broken lines) or to $\gamma'' + \gamma'$ (solid lines).

measurements on a polished sections), precipitate agglomeration/encounter during the latter stages of aging,[47,48] or other effects neglected in the analysis.

The comparison of predictions from the nucleation-and-growth simulations also showed moderate-to-good agreement with precipitation trends inferred from neutron-diffraction lattice-parameter measurements (Figure 9). In these instances, the normalized predictions were plotted for both the total ($\gamma'' + \gamma'$) volume fraction as well as for γ'' alone, the latter being the more appropriate case. For an aging temperature of 953 K, both simulation results appeared to be bounded by the scatter in the experimental data (Figure 9(a)). For the comparison at 1053 K (Figure 9(b)), both simulation trends indicated kinetics slower than those observed, with the difference being greater for the γ''-alone simulation. This trend contrasted with that for DRM for which the 1053 K simulation prediction suggested comparable or slightly faster kinetics than those observed (Figure 7(d)). Despite such differences, it can be concluded that both DRM and neutron diffraction provide a useful tool to estimate precipitation behavior for superalloy 718 to a good first order.

V. FUTURE PERSPECTIVES

The present work has introduced two novel techniques to measure the precipitation kinetics of 718 and related superalloys such as 625.[49] Both techniques show great promise for industrial and fundamental-research applications. Improvements in the techniques may enhance their attractiveness, however. Key among these perhaps is the ability to rapidly heat/cool samples. Such a capability would eliminate the confounding influence of moderate heating rate per se in the interpretation of otherwise isothermal kinetic behavior. It would also enable more reliable measurements of the cooling-transformation behavior of 718 for which noticeable variations are found in the literature. Rapid *in-situ* techniques such as DRM and ND may also enable rapid quantification of the effect of variations in alloy composition on aging kinetics.

The advent of *in-situ* experimental techniques for aging problems may also spur modeling-and-simulation research for complex alloys such as 718. For example, research to quantify important thermodynamic parameters (*e.g.*, phase compositions/phase fractions and descriptions of the Gibbs free-energy as function of temperature) is greatly needed.[44,50]

VI. SUMMARY AND CONCLUSIONS

Two different *in-situ* experimental techniques, one based on the dynamic-resonance method (DRM) and the other on neutron diffraction, were investigated to determine their suitability to measure precipitation kinetics for superalloy 718 at temperatures between 923 K and 1053 K. Based of this research, the following conclusions were drawn:

1. The temporal variation of Young's modulus can be quantitatively related to the evolution of γ'' and γ' precipitates during the aging of solution-treated superalloy 718. DRM thus provides a rapid and inexpensive alternative to establish transformation kinetics compared to *ex-situ* heat treatments followed by high-magnification transmission or scanning electron microscopy. The present results also suggest measurably-higher elastic moduli for γ''/γ' than heretofore reported in the literature.
2. Tracking of the evolution of the γ-matrix lattice parameter *via* neutron diffraction also yields a semi-quantitative measure of precipitation behavior, much like DRM. The technique tends to complement DRM inasmuch as it is based on the misfit strains developed between the γ marix and largely the γ'' precipitates alone.
3. From a phenomenological standpoint, the precipitation kinetics deduced from DRM and neutron diffraction exhibit a transition in Avrami exponent from higher to lower values with increasing

temperature in the range of 923 K to 1053 K. In concert with corroborating nucleation-and-growth simulations, the observations thus provide support for a transition from nucleation-controlled to growth-controlled behavior typically used to explain the overall shape of isothermal-transformation diagrams such as those for superalloy 718.

4. To a first order, the isothermal precipitation kinetics observed for 718 using DRM or neutron diffraction are predicted well by numerical simulations based on classical models of homogeneous nucleation and diffusional growth.

ACKNOWLEDGMENTS

Portions of this work were conducted as part of the in-house research of the Air Force Research Laboratory's Materials and Manufacturing Directorate. Encouragement from and discussions with W. Cao, T.P. Gabb, T.A. Parthasarathy, D.F. Paulonis, and R.A. Thomas are very much appreciated. The authors are also grateful for the allocation of beam time (per RB2000109) at the ENGIN-X, ISIS, facility, Rutherford Appleton Laboratory and to Dr. T-L. Lee for his yeoman support during the neutron-diffraction experiments. Last, Safran Aircraft Engines (Dr. Jean Mériaux) is sincerely thanked for providing a portion of the material used for this research endeavor.

APPENDIX: EFFECT OF CONTINUOUS HEATING ON PRECIPITATION

Unlike the rapid heating to test temperature utilized in the neutron-diffraction experiments, the DRM equipment design and associated test method mandated a slow heating rate to the desired test temperature(s). Hence, N&G simulations incorporating the specific heating rate prior to soaking were conducted to quantify the effect of such thermal transients on subsequent precipitation at the soak/peak temperature per se. In all of these simulations, the baseline material coefficients (Table II) and a heating cycle comprising a constant ramp rate of 2 K/min from 873 K to the test temperature were used.

Simulation results for test temperatures of 923 K and 953 K indicated that the initial heat-up had essentially no effect on subsequent aging behavior. For 953 K, for example, the predicted volume fractions of precipitates upon reaching test temperature were ~ 0.00004 (γ'') and ~ 0.0009 (γ').

As shown in Figure A.1(a), predictions for a peak/test temperature of 1013 K showed a small effect of the initial heating transient (occurring at times $t \leq 0$, for which the soak period was defined to begin at $t = 0$). Here, the simulation prediction without the heat-up effect (smooth black curve) and the experimental results (data points) are reproduced from Figure 7(c). Simulation predictions incorporating the heating cycle are shown as smooth curves which are green (normalized $\gamma'' + \gamma'$ volume fraction) or brown (normalized γ'' volume fraction).

Although ~ 1/10 of the total precipitate fraction produced under long-time soaking at the peak temperature was predicted to evolve during heating to 1013 K, the overall trends were very similar to those for the prediction for which the heating cycle was neglected (black curve). That is to say, the green and black curves were quite similar to each other except for $t \leq 0.35$ hours.

The comparison for the highest test temperature (1053 K, Figure A.1(b)) showed a noticeable effect of the heating ramp on aging response. In this instance, ~ 40 pct of the equilibrium volume fraction of precipitate at this temperature was predicted to have been produced during heat-up. Despite the marked difference between the isothermal simulation (black curve) and those

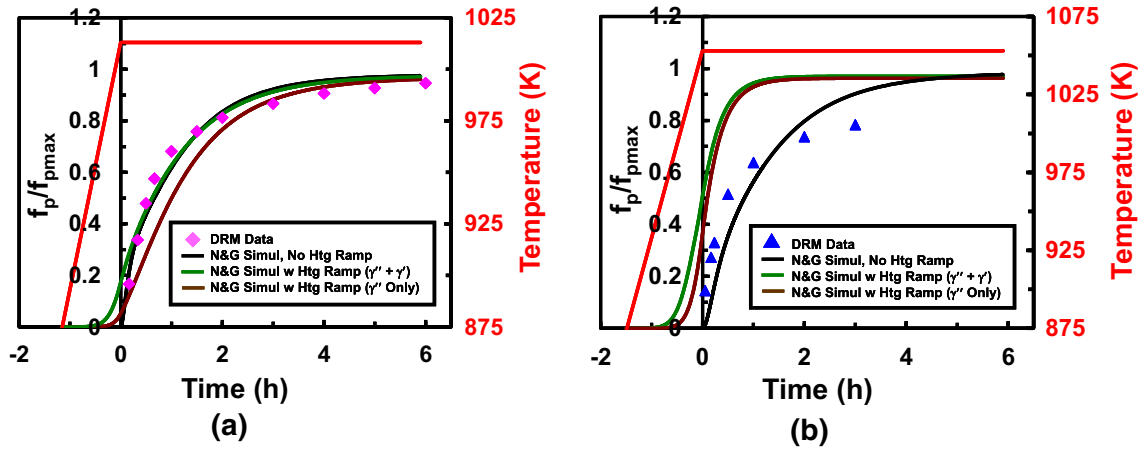

Fig. A.1—Comparison of DRM measurements (data points) and isothermal N&G simulation predictions (black curves) to N&G simulations incorporating a heating ramp from 873 K (smooth green, brown curves) for peak/test temperatures of: (*a*) 1013 K or (*b*) 1053 K (Color figure online).

including the heating ramp (green curve for the normalized $\gamma'' + \gamma'$ volume fraction and brown curve for the normalized γ'' volume fraction), all of the simulations did indicate a similar sharp initial rise during the first hour of aging at the peak temperature. Nevertheless, the transient simulations do bring into question the key assumption of no precipitates (and thus no enhancement of the measured modulus) at the start of the soak, which was used to analyze the present DRM measurements. To account for this shortcoming at least partially, the transient predictions for $t \geq 0$ were rescaled to lie between 0 and unity in an attempt to mimic the erroneous assumption used for the DRM analysis. Agreement between the experimental data and the curves so adjusted (not shown) was improved only slightly, however. Such comparisons for 1053 K are not surprising in view of the heating transient passing through the nose of TTT curves, which lie at ~ 1020 to 1050 K. Moreover, this finding likely confounds the interpretation of the JMAK plot for 1053 K (shown in Figure 6(d)) as well, and merits further investigation.

REFERENCES

1. H.L. Eiselstein: in *Advances in the Technology of Stainless Steel and Related Alloys*, *ASTM STP 369*, American Society for Testing and Materials, Philadelphia, 1965, pp. 62–79.
2. R.E. Schafrik, D.D. Ward, and J.R. Groh: in *Superalloys 718, 625, 706, and Various Derivatives*, E.A. Loria, ed., TMS, Warrendale, PA, 2001, pp. 1–11.
3. D. Paulonis and J.J. Schirra: in *Superalloys 718, 625, 706, and Various Derivatives*, E.A. Loria, ed., TMS, Warrendale, PA, 2001, pp. 13–23.
4. J.A. Heaney, M.L. Lasonde, A.M. Powell, B.J. Bond, and C.M. O'Brien: in *Proceedings of 8th International Symposium on Superalloy 718 and Derivatives*, E. Ott, A. Banik, X. Liu, I. Dempster, K. Heck, J. Andersson, J. Groh, R. Helmink, and A. Wusatowski-Sarnek, eds., 2014, TMS, Warrendale, PA, pp. 67–77.
5. *Proceedings of 9th International Symposium on Superalloy 718 and Derivatives*, E. Ott, X. Liu, J. Andersson, Z. Bi, K. Bockenstedt, I. Dempster, J. Groh, K. Heck, P. Jablonski, M. Kaplan, D. Nagahama, and C. Sudbrack, eds., 2018, TMS, Pittsburgh, PA, 2018.
6. Y.C. Fayman: *Mater. Sci. Eng.*, 1987, vol. 92, pp. 159–71.
7. J.W. Brooks and P.J. Bridges: in *Superalloys 1988*, S. Reichman, D.N. Duhl, G. Mauer, S. Antolovich, and C. Lund, eds., TMS, Warrendale, PA, 1988, pp. 33–42.
8. A. Oradei-Basile and J.F. Radovich: in *Superalloys 718, 625, and Various Derivatives*, E.A. Loria, ed., TMS, Warrendale, PA, 1991, pp. 325–35.
9. C.I. Garcia, D.E. Camus, E.A. Loria, and A.J. DeArdo: in *Superalloys 718, 625, and Various Derivatives*, E.A. Loria, ed., TMS, Warrendale, PA, 1991, pp. 925–41.
10. C.I. Garcia, A.K. Lis, E.A. Loria, and A.J. DeArdo: in *Superalloys 1992*, S.D. Antolovich, R.W. Stusrud, R.A. MacKay, D.L. Anton, T. Khan, R.D. Kissinger, and D.L. Klarstrom, eds., TMS, Warrendale, PA, 1992, pp. 527–36.
11. H. Chandler: *Heat Treater's Guide: Practices and Procedures for Nonferrous Alloys*, ASM International, Materials Park, OH, 1996.
12. C. Slama and G. Cizeron: Etude du Comportement Structural de l'Alliage NC 19 Fe Nb (Inconel 718)*J. Phys. III*, 1997, vol. 7, pp. 665–88.
13. A. Thomas, M. El-Wahabi, J.M. Cabrera, and J.M. Prado: *J. Mater. Proc. Technol.*, 2006, vol. 177, pp. 469–72.
14. R. Cozar and P. Pineau: *Metall. Trans.*, 1973, vol. 4, pp. 47–59.
15. M. Sundararaman, P. Mukhopadhyay, and S. Banerjee: *Metall. Trans. A*, 1992, vol. 23A, pp. 2015–28.
16. Y.F. Han: M.S. Thesis, University of Manitoba, Winnipeg, Manitoba, Canada, 1981.
17. R.Y. Zhang, H.L. Qin, Z.N. Bi, J. Li, S. Paul, T.L. Lee, B. Nenchev, J. Zhang, S. Kabra, J.F. Kelleher, and H.B. Dong: *Metall. Mater. Trans. A*, 2019, vol. 50A, pp. 5421–32.
18. R. Lawitzki, S. Hassan, L. Karge J. Wagner, D. Wang, J. von Kobylinski, C. Krempaszky, M. Hofmann, R. Gilles, and G. Schmitz: *Acta Mater.*, 2019, vol. 163, pp. 28–39.
19. F. Theska, S.P. Ringer, and S. Primig: *Microsc. Microanal.*, 2019, vol. 25, pp. 470–80.
20. T.M. Smith, N.M. Senanayake, C.K. Sudbrack, P. Bonacuse, R.B. Rogers, P. Chao, and J. Carter: *Mater. Charact.*, 2019, vol. 148, p. 78.
21. R.Y. Zhang, H.L. Qin, Z.N. Bi, J. Li, S. Paul, T.L. Lee, S.Y. Zhang, J. Zhang, and H.B. Dong: *Metall. Mater. Trans. A*, 2020, vol. 51A, pp. 574–85.
22. A. Niang: Ph.D. Thesis, Université de Toulouse, Toulouse, France, 2010.
23. A. Niang, B. Viguier, and J. Lacaze: *Mater. Characterization*, 2010, vol. 61, pp. 525–34.
24. K. Wu, F. Zhang, S. Chen, W. Cao, and Y.A. Chang: in *Superalloys 2008*, R.C. Reed, K.A. Green, P. Caron, T.P. Gabb, M.G. Fahrmann, E.S. Huron, and S.A. Woodard, eds., TMS, Warrandale, PA, 2008, pp. 933–39.
25. F. Zhang, W. Cao, C. Zhang, S. Chen, J. Zhu, and D. Lv: in *Proc. 9th International Symposium on Superalloy 718 and Derivatives*, E.A. Ott, ed., TMS, Pittsburgh, PA, 2018, pp. 147–61.
26. A. Drexler, B. Oberwinkler, S. Primig, C. Turk, E. Povoden-Karadeniz, A. Heinemann, W. Ecker, and M. Stockinger: *Mater. Sci. Eng. A*, 2018, vol. A723, pp. 314–23.
27. Z.K. Low, T. Chaise, D. Bardel, S. Cazottes, P. Chaudet, M. Perez, and D. Nelias: *Acta Mater.*, 2018, vol. 156, pp. 31–42.
28. I.J. Moore, M.G. Burke, and E.J. Palmiere: *Acta Mater.*, 2016, vol. 119, pp. 157–66.
29. P. Mazot, J. de Fouquet, J. Woirgard, and J.P. Pautrot: *J. Phys. III*, 1992, vol. 2, pp. 751–63.
30. L. Barboni, G.R. Gillich, C.P. Chioncel, C.O. Hamat, and I.C. Mituletu: in *IOP Conf. Series: Mater. Sci. Eng.*, 2018, vol. 416, paper 012063.
31. G. Leon and H.L. Chen: *Vibration*, 2019, vol. 2, pp. 157–73.
32. *ASTM Standard E1875-13*, ASTM Inter., Conshohocken, PA, 2014.
33. P.E. Aba-Perea, T. Pirling, P.J. Withers, J. Kelleher, S. Kabra, and M. Preuss: *Mater. Des.*, 2016, vol. 89, pp. 856–63.
34. S.V. Prikhodko, J.D. Carnes, D.G. Isaak, H. Yang, and A.J. Ardell: *Metall. Mater. Trans. A*, 1999, vol. 30A, pp. 2403–08.
35. J. Santisteban, M. Daymond, J. James, and L. Edwards: *J. Appl. Crystallogr.*, 2006, vol. 39, pp. 812–25.
36. J.W. Christian: *The Theory of Transformation in Metals and Alloys*, Pergamon Press, Oxford, UK, 2002.
37. M. Akhlaghi, T. Steiner, S.R. Meka, and E.J. Mittemeijer: *J. Appl. Crystall.*, 2016, vol. 49 (1), pp. 69–77.
38. A.N. Kolmogorov: *Izv. Akad. Nauk. SSSR, Ser. Materm.*, 1937, vol. 3, pp. 335–59.
39. W.A. Johnson and R.F. Mehl: *Trans. AIME*, 1939, vol. 135, pp. 416–43.
40. M. Avrami: *J. Chem. Phys.*, 1939, vol. 7, pp. 1103–1112.
41. M. Avrami: *J. Chem. Phys.*, 1940, vol. 8, pp. 212–224.
42. M. Avrami: *J. Chem. Phys.*, 1941, vol. 9, pp. 177–84.
43. R. Wagner and R. Kampmann: in *Materials Science and Technology*, vol. 5, P. Haasen, ed., VCH, Weinheim, Germany, 1991, pp. 213–303.
44. S.L. Semiatin, J.S. Tiley, F. Zhang, T.M. Smith, R.Y. Zhang, H.B. Dong, P. Gadaud, and J. Cormier: *Metall. Mater. Trans. A*, 2020 (accepted for publication).
45. D.F. Paulonis, J.M. Oblak, and D.S. Duvall: *Trans. ASM*, 1969, vol. 62, pp. 611–22.
46. A. Devaux, L. Naze, R. Molins, A. Pineau, A. Organista, J.Y. Guedou, J.F. Uginet, and P. Heritier: *Mater. Sci. Eng. A*, 2008, vol. A486, pp. 117–22.
47. I.J. Moore, M.G. Burke, N.T. Nuhfer, and E.J. Palmiere: *J. Mater. Sci.*, 2017, vol. 52, pp. 8665–80.

48. A. Seret, C. Moussa, M. Bernacki, and N. Bozzolo: *Acta Mater.*, 2020, vol. 192, pp. 40–51.
49. L. Mataveli Suave, J. Cormier, P. Villechaise, A. Soula, Z. Hervier, D. Bertheau, and J. Laigo: *Metall. Mater. Trans. A*, 2014, vol. 45A, pp. 2963–82.
50. D. Furrer, V. Venkatesh, F. Zhang, D. Gynther, T. Asare, D. Novikov, and S. Burlatsky: in *Proc. 8th Inter. Symp. on Superalloy 718 and Derivatives*, E. Ott, A. Banik, X. Liu, I. Dempster, K. Heck, J. Andersson, J. Groh, R. Helmink, and A. Wusatowska-Sarnek, eds., 2014, TMS, Warrendale, PA, pp. 81–94.